ACS OMEGA

http://pubs.acs.org/journal/acsodf

Article

Orange Pomace-Derived Fluorescent Carbon Quantum Dots: Detection of Dual Analytes in the Nanomolar Range

Aayushi Kundu, Banibrata Maity,* and Soumen Basu*

Cite This: *ACS Omega* 2023, 8, 22178−22189

Read Online

ACCESS | Metrics & More | Article Recommendations | Supporting Information

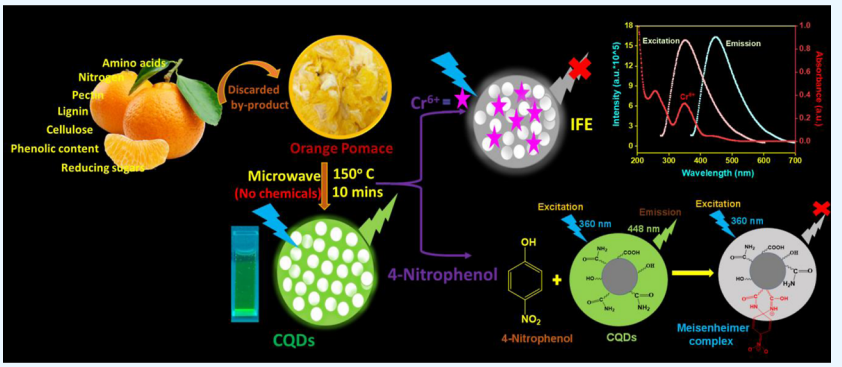

ABSTRACT: Green-emissive carbon quantum dots (CQDs) with exclusive chemosensing aspects were synthesized from orange pomace as a biomass-based precursor *via* a facile microwave method without using any chemicals. The synthesis of highly fluorescent CQDs with inherent nitrogen was confirmed through X-ray diffraction, X-ray photoelectron, Fourier transform infrared, Raman, and transmission electron microscopic techniques. The average size of the synthesized CQDs was found to be 7.5 nm. These fabricated CQDs displayed excellent photostability, water solubility, and outstanding fluorescent quantum yield, *i.e.*, 54.26%. The synthesized CQDs showed promising results for the detection of Cr^{6+} ions and 4-nitrophenol (4-NP). The sensitivity of CQDs toward Cr^{6+} and 4-NP was found up to the nanomolar range with the limit of detection values of 59.6 and 14 nM, respectively. Several analytical performances were thoroughly studied for high precision of dual analytes of the proposed nanosensor. Various photophysical parameters of CQDs (quenching efficiency, binding constant, *etc.*) were analyzed in the presence of dual analytes to gain more insights into the sensing mechanism. The synthesized CQDs exhibited fluorescence quenching toward incrementing the quencher concentration, which was rationalized by the inner filter effect through time-correlated single-photon counting measurements. The CQDs fabricated in the current work exhibited a lower detection limit and a wide linear range through the simple, eco-friendly, and rapid detection of Cr^{6+} and 4-NP ions. To evaluate the feasibility of the detection approach, real sample analysis was conducted, demonstrating satisfactory recovery rates and relative standard deviations toward the developed probes. This research paves the way for developing CQDs with superior characteristics utilizing orange pomace (biowaste precursor).

INTRODUCTION

Carbon quantum dots (CQDs) are a distinct group of fluorescent nanomaterials with a diameter of less than 10 nm, which have gained prominence in recent years.[1] CQDs are carbonaceous nanomaterials that are quasi-spherical in shape with sp^2 carbon and oxygen-containing groups.[2] They possess unique physiochemical properties like stable photoluminescence (PL), versatile surface chemistry, excellent hydrophilicity, biocompatibility,[3] low toxicity, excitation wavelength-dependent emission, and eco-friendly nature.[4] CQDs can be used in a plethora of applications like sensing,[5] solar cells, bio-imaging, bio-electrochemistry,[6] nanomedicine,[7] and photocatalysis.[8] A thorough review of the available literature found that organic compounds and natural precursors (biomass and biowaste) were employed to synthesize CQDs.[9] Organic compounds like citric acid, glycerol, and chitosan have been used to produce CQDs but have limitations like toxicity, post-surface passivation, and harsh reaction conditions.[9] Therefore, it is preferable to synthesize CQDs through eco-friendly, affordable, and facile pathways from biomass.[10] Biomass-derived CQDs have high C content (45−55 wt %).[11] Also, this is the cost-efficacious and convenient method for the mass production of CQDs without involving any refractory solvents.[11]

Received: April 12, 2023
Accepted: May 26, 2023
Published: June 6, 2023

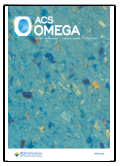

Supercritical water can be used for green synthesis/extraction of the total organic carbon content of wastes. The distinctive characteristics of supercritical water, such as its low dielectric constant, high specific heat capacity, and high pressure, enable the active involvement of supercritical water molecules in the cleavage of chemical bonds by lowering the activation energy. This supercritical water also helps in getting a higher yield of quantum dots.[12] Using subcritical water, an extensive range of environmentally friendly materials can be extracted from various bio-wastes and agricultural byproducts.[13]

Despite the progress in selecting green carbon precursors like apple juice,[14] garlic,[15] orange juice,[16] and lemon juice,[17] the use of edible products continues to be a challenge.[18] The more favorable choice is to use the agro-industrial waste that comes from the consumption of primary products.[19,20] The beverage and juice industries generate ∼125 million tonnes of by-products.[21] *Citrus sinensis* (orange) is the typical citrus fruit with a global production of ∼73 million tonnes used for non-culinary and culinary purposes.[18] After juice production, the byproduct formed is known as pomace, often discarded. Each year, ∼15 million tonnes of orange juice byproducts are generated globally.[22] Orange pomace contains amino acids, nitrogen, reducing sugars, fat (low content), pectin, cellulose, lignin, moisture, nucleic acid, and phenolic content.[21] Interestingly, pomace can be an effective green precursor for CQDs synthesis. Also, microwave irradiation used in the synthesis process might induce the formation of local super/sub-critical water in the porous materials of the wastes.

The inherent N functionalities and surface-bound functional groups like phenolic, carboxyl, *etc.*, in the as-prepared CQDs were responsible for the sensing of different analytes.

Meanwhile, chromium (Cr) is one of the heavy metal pollutants affecting human health and the environment.[23] Among all the forms, Cr(VI) has drawn attention in recent times as it causes hereditary gene defects, allergic reactions, nasal mucosal irritation, and cancers.[24] The United States Environmental Protection Agency identified it as a heavy metal pollutant in the atmosphere.[25] Therefore, rapid and accurate Cr(VI) detection is of utmost importance. Also, 4-nitrophenol (4-NP) is one of the refractory and noxious pollutants in the effluents produced from the manufacture of pharmaceutical dyes, explosives, and agrochemicals. The ingestion of 4-NP could lead to disorders like headache, kidney and liver damage, and methemoglobinemia.[26] Owing to its carcinogenic capacity and toxicity, the U.S. EPA has listed it in the "primary pollutant list".[27] Hence, it is vital to create a very specific and sensitive detection system for the detection of 4-NP to save the environment and public health. Cr(VI) and 4-NP can be detected using various techniques such as chromatography,[28,29] atomic absorption spectroscopy,[30] colorimetry,[31,32] ion exchange,[33,34] and electrochemical method.[35,36] However, these methods have certain shortcomings like long operation time, complex sample pre-treatment, and expensive equipment.[37] Fluorescence spectroscopy is a widely used technique because of its cost-effectiveness, excellent sensitivity, high selectivity, and quick response time.[38] *Wang and co-workers* fabricated N-doped CQDs from a chelating agent and used it for detecting Cr(VI) ions.[39] *Xu et al.* prepared N-doped CQDs from D-glucose and L-arginine, which were used to detect Fe(III) and Cr(VI).[40] *Guo et al.* described the hydrothermal preparation of N- and B-doped carbon dots for sensing Cr(VI) through a fluorescence quenching mechanism.[41] *Mondal et al.* prepared CQDs using citric acid and lanthanide to detect Cr(VI).[42] *Li et al.* employed apple peels for CQD synthesis and utilized it for the detection of Cr(VI) having a detection limit, *i.e.*, 0.73 μM.[43] Das and Dutta synthesized N-doped carbon dots with ethylene glycol and β-alanine for the detection of 4-NP and Cr(VI) with the 0.4 and 0.29 μM detection limit, respectively.[44] Huang reported the sensitive detection of 4-NP having 0.05 μM detection limit using cuttlefish ink-based N and S co-doped CQDs.[45] Amjadi and Hallaj studied a glucose-derived CQD−$Ru(bpy)_3^{2+}$−Ce(IV) chemiluminescence sensor designed for the determination of 4-NP.[46]

This study emphasizes on synthesizing CQDs using orange pomace through the one-pot facile, green, and microwave-assisted methods without the incorporation of any chemicals. The as-prepared CQDs showed green emission and highly fluorescence property. The developed sensor was used for the selective and sensitive detection of Cr^{6+} and 4-NP at the nanomolar level by an inner filter mechanism. This study also validates the results of real sample analysis.

EXPERIMENTAL SECTION

Materials. Orange pomace was taken from a local juice shop (Patiala, India). All the chemicals necessary to prepare metal ion stock solutions were acquired from Loba Chemie, India. Deionized (DI) water was utilized during the experiments.

Synthesis of Orange Pomace-Derived CQDs. To begin, the orange pomace was gently cleansed with DI water. Water (100 mL) was added to pomace and grinded in a mixer which was further filtered, and juice was collected. The filtered juice was transferred to a reaction vial and kept for heating at 150 °C (300 W) for 10 min in a microwave reactor. The obtained solution was filtered using a syringe filter (0.22 μm) to obtain brown-colored CQDs as illustrated in Scheme 1.

Scheme 1. Synthesis of CQDs from Orange Pomace

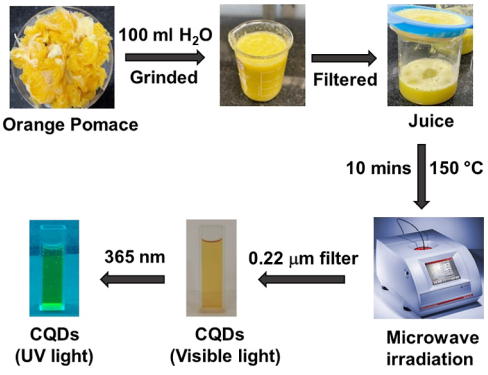

Sample Solution Preparation. The standard solution (1 mM) of various metals (cations: Co^{2+}, Fe^{3+}, Cr^{6+}, Cu^{2+}, Ni^{2+}, Fe^{2+}, Zn^{2+}, Al^{3+}, Cr^{3+}, Hg^{2+}, Pb^{2+}, and Cd^{2+} and anions: ClO_3^-, PO_4^{3-}, NO_2^-, SO_4^{2-}, Cl^-, NO_3^-, OH^-, F^-, and S^{2-}) and analytes [glucose, hydroquinone (HQ), ascorbic acid (AA), 4-NP, 2-nitrophenol (2-NP), glycine, ethylenediaminetetraacetic acid (EDTA), alanine, glutathione, methoxy phenol (MP), nitrobenzene, 1-fluoro 2-nitrobenzene, and phenol] were made in DI water to perform the selectivity experiments of the synthesized CQDs. 0.1 mM solution was pipetted into the cuvette with the addition of 10 μL of CQDs in 2 mL of DI water. Further, the sensitivity study validation was carried out using a 1 μM stock solution of Cr(VI) and 4-NP.

https://doi.org/10.1021/acsomega.3c02474
ACS Omega 2023, 8, 22178−22189

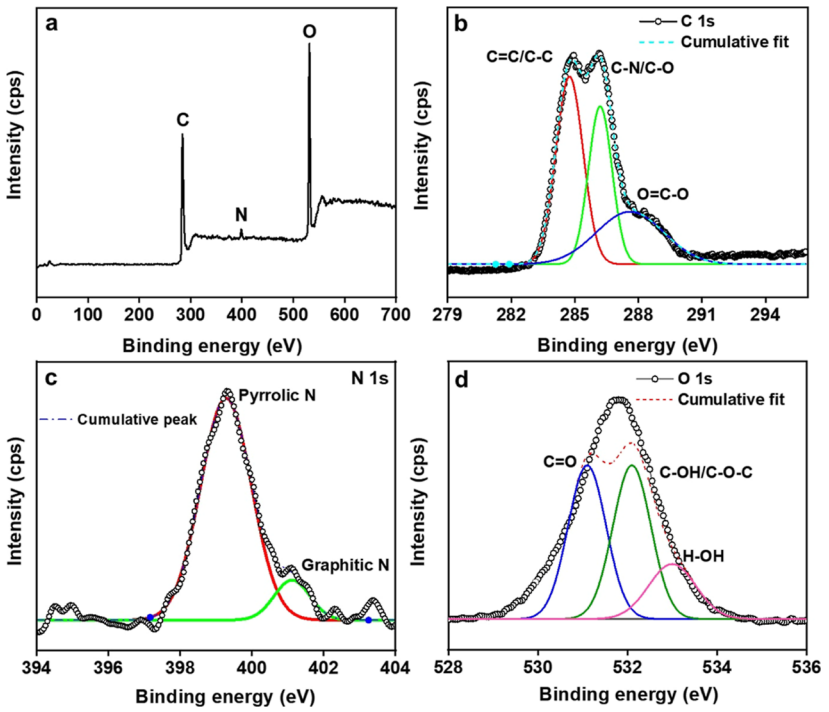

Figure 1. (a) Survey spectra of CQDs and (b) high-resolution spectra of C 1s, (c) N 1s, and (d) O 1s of CQDs.

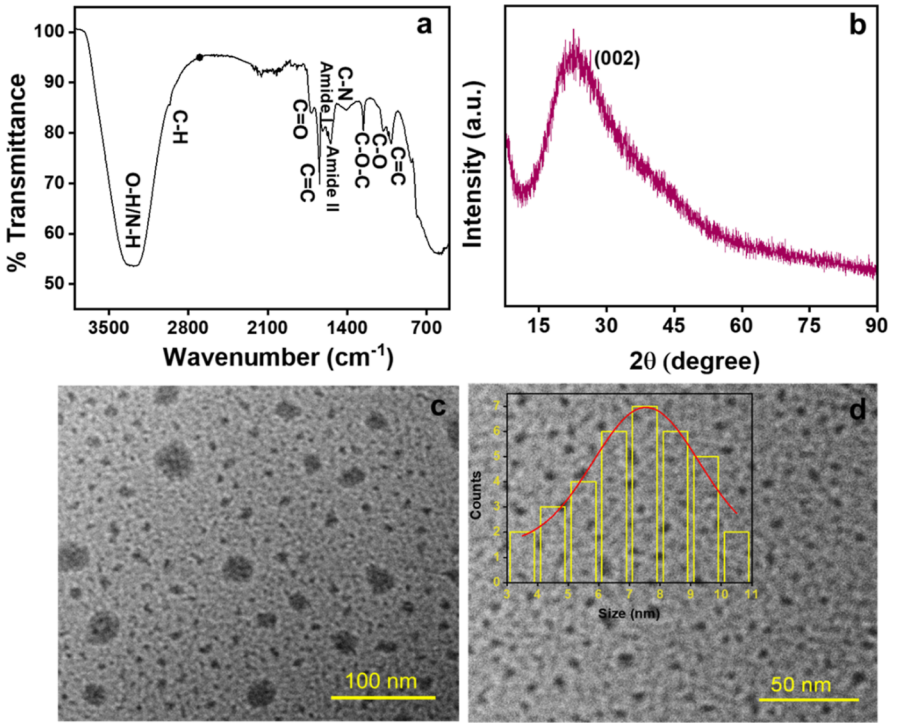

Figure 2. (a) FT-IR graph of CQDs, (b) XRD spectra, and (c,d) TEM images with the inset showing the size distribution histogram of CQDs.

Real Sample Analysis. To examine the applicability of the present sensing method, the experiment was conducted with real samples (lake water and tap water). The water samples were collected from Patiala, India. Prior to analysis, the water samples underwent filtration using 0.45 μm nylon filters. After spiking the samples with different concentrations of Cr^{6+} and 4-NP, a solution of CQDs was added, and fluorescence measurements were recorded at a wavelength of 360 nm.

Quantum Yield Measurements. The fluorescence quantum yields of CQDs in the existence of Cr(VI) and 4-NP were measured with quinine sulfate[47] solution as a reference (ϕ_R = 0.546) from eq 1

$$\phi_S = \phi_R \times \frac{A_S}{A_R} \times \frac{(Abs)_R}{(Abs)_S} \times \frac{\eta_S^2}{\eta_R^2} \quad (1)$$

https://doi.org/10.1021/acsomega.3c02474
ACS Omega 2023, 8, 22178−22189

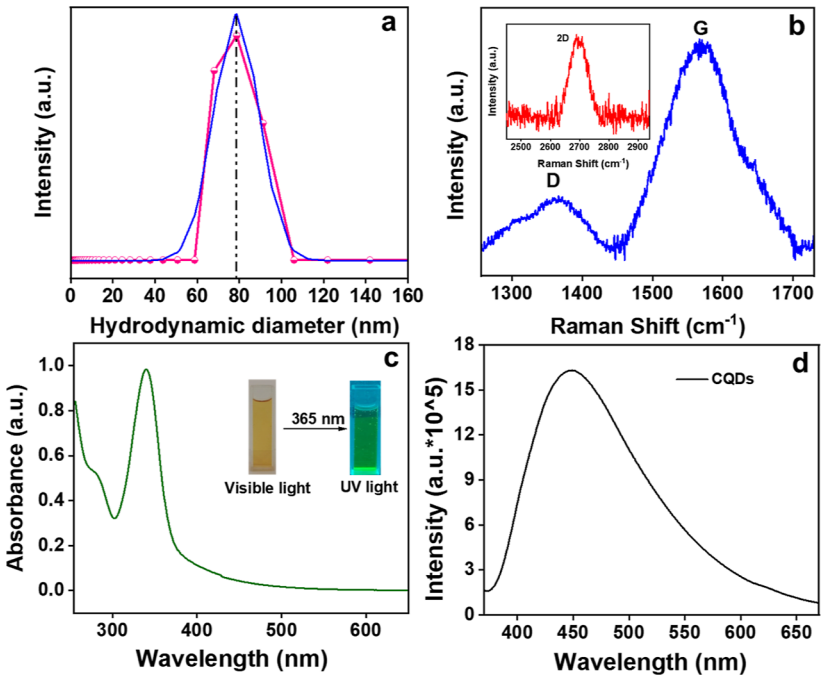

Figure 3. (a) DLS size distribution, (b) Raman spectra of CQDs with the inset showing the 2D band, (c) UV−vis absorption spectrum with the inset showing CQDs exposed to visible and ultraviolet light, and (d) fluorescence emission spectrum of the as-prepared CQDs.

"ϕ_S" refers to the samples' quantum yield and "ϕ_R" denotes the quantum yield of the reference solution. "Abs", "A", and "η" refers to the absorbance, emission area, and refractive index, respectively.

RESULTS AND DISCUSSION

Characterization. X-ray photoelectron spectroscopy (XPS) study was done to know the surface chemical composition of the synthesized CQDs. The survey spectra exhibit peaks at 283.8, 398.5, and 531.6 eV corresponding to C 1s (66.68%), N 1s (2.45%), and O 1s (30.87%), respectively (Figure 1a). The high-resolution C 1s spectrum (Figure 1b) shows three major peaks at 284.8, 286.1, and 287.4 eV ascribing to C═C/C−C, C−O/C−N, and O═C−O, respectively.[48] The N 1s spectrum (Figure 1c) exhibits peaks at 399.3 and 401.1 eV corresponding to N−H and C−N, respectively.[49] The O 1s spectrum (Figure 1d) showed peaks at 531.1, 532.1, and 533.0 eV assigned to C═O, C−O−C/C−OH, and H−OH, respectively, with the 25% water content in the sample.[50] The functional groups on the CQD surface were confirmed through Fourier transform infrared (FT-IR) spectroscopy (Figure 2a). The FT-IR absorption bands were observed at 3352 cm^{-1} ascribed to the stretching vibration of the O−H/N−H group. A small band at 2961 cm^{-1} resembles C−H stretching vibration, and signals at 1737 and 1622 cm^{-1} correspond to C═O and C═C stretching, respectively. Additionally, peaks for amide II at 1571 cm^{-1} and amide I at 1618 cm^{-1} correspond to the bending vibration of amide confirming the amide bonds.[51] The band at 1480 cm^{-1} corresponds to C−N stretching. Peaks at 1258 and 1087 cm^{-1} confirm the C−O stretching.[50] The signal at 1008 cm^{-1} corresponds to C═C bending vibrations. This affirmed the presence of hydroxyl, carboxyl, and amino groups on the CQD surface. The zeta potential was −12.6 mV, confirming the abundance of negatively charge functional groups on CQDs (Supporting Figure S1a).[52] The X-ray diffraction (XRD) spectrum (Figure 2b) showed that the broad amorphous peak at $2\theta = 23.5°$ was attributed to the (002) graphitic carbon lattice spacing of the as-prepared CQDs.[43,52]

The size and morphology of the orange pomace-derived CQDs were analyzed using transmission electron microscopy (TEM). Figure 2c,d shows that the as-prepared CQDs are nearly spherical in shape. The inset of Figure 2d exhibits the particle size histogram distribution ranging from 3 to 11 nm, with a computed average particle size of 7.5 nm. The hydrodynamic particle size (∼78 nm) was calculated using the DLS data (Figure 3a). Figure 3b exhibits the Raman spectrum depicting two peaks at 1360 cm^{-1} (disordered-D) and 1568 cm^{-1} (graphite-G) bands.[53] The G band is a result of the first-order scattering of E_{2g} phonons from carbon atoms that are sp^2-hybridized, while the D band arises due to a breathing motion of κ-point phonons with the A_{1g} symmetry associated with defects in the sp^3 carbon bonds, like hydroxyl and/or epoxide bonds.[54] The higher intensity of the G band showed the presence of sp^2 carbons with fewer sp^3-hybridized carbon atoms in the synthesized CQDs. The additional wide 2D band seen at around 2694 cm^{-1} showed the sp^2 hybridization (second-order phonon process).[55,56] The 2D band, historically known as G′, represents an overtone of the D band.[57]

Optical Property Analysis. The optical properties were studied using UV−vis spectra and the PL emission spectrum. Figure 3c depicts a predominant absorption band at 340 nm for C═O credited to n−π^* and a weak absorption band at 275 nm due to the $\pi-\pi^*$ transition of sp^2 domains of the carbon core.[58] The inset image showed a brown color during visible light irradiation and emits green fluorescence on irradiation of UV light (365 nm). This is ascribed to radiative recombination among electrons and holes, which is due to the photoinduced separation of charge and surface site trapping, leading to PL emission of the fabricated CQDs.[59] The PL emission spectra are shown in Figure 3d. The highest emission peak was observed at 448 nm upon excitation of 360 nm. The high PL quantum yield of 54.26% was noticed for the as-prepared CQDs. A bath-

https://doi.org/10.1021/acsomega.3c02474
ACS Omega 2023, 8, 22178−22189

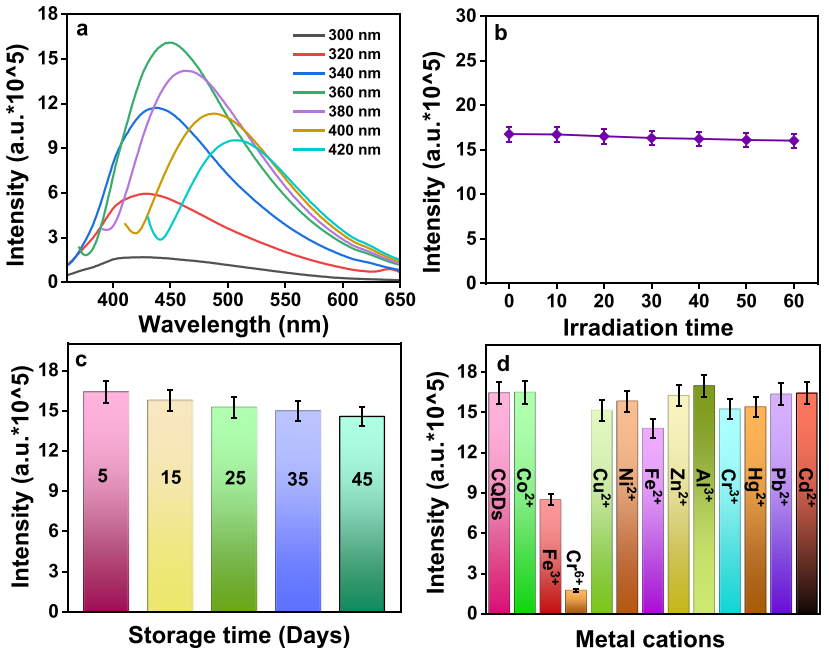

Figure 4. (a) Spectra of PL emission at different excitation wavelengths, (b) impact of time (min), (c) effect of storage duration (days) on CQDs PL stability, and (d) CQDs selectivity tests using various metal cations.

ochromic shift (Figure 4a) is noticed in the emission wavelength from 417 to 506 nm with a change in excitations at 300−420 nm. This excitation-dependent fluorescence emission of CQDs is related to fluorescence excitation energy and different factors like quantum confinement effect, surface edge defects, sp^2 π domains, zigzag edge sites, and size variation.[59]

Stability Studies of CQDs. The stability of CQD luminescence properties is a vital factor to be considered prior to further applications. The role of pH and irradiation time on the PL intensity of CQDs was studied. To know the photostability, the as-prepared CQDs were irradiated under a Xe lamp for 60 min, and no substantial change in intensity was seen (Figure 4b). CQDs were also stored for 45 days, and the fluorescence spectra were taken at regular intervals, revealing no discernible change in PL intensity over the course of time (Figure 4c). It affirms the high stability of CQDs. Additionally, the effect of pH (3−13) was investigated to know the pH interference with the PL intensity of CQDs. At various pH, almost the same PL intensity of CQDs was observed, proving that CQDs can work effectively in both acidic and basic environments[60] (Figure S1b).

Selectivity Studies for Cr(VI). This is an important parameter to study while developing a potent sensor. The variation in the PL intensity of the CQDs with 0.1 mM concentration of the stock solution of different metal cations (Co^{2+}, Fe^{3+}, Cr^{6+}, Cu^{2+}, Ni^{2+}, Fe^{2+}, Zn^{2+}, Al^{3+}, Cr^{3+}, Hg^{2+}, Pb^{2+}, and Cd^{2+}) was studied. The result indicated a significant PL response after the addition of Fe^{3+} and Cr^{6+} ions, while all other cations show minimal response (Figure 4d). To further confirm the selectivity of the CQDs toward anions, its fluorescence behavior in the presence of different anions (ClO_3^-, PO_4^{3-}, NO_2^-, SO_4^{2-}, Cl^-, NO_3^-, OH^-, F^-, and S^{2-}) was also considered. The results exhibited that there is negligible response on the CQD intensity on varying the anions (Figure S2). However, Cr^{6+} showed the maximum fluorescence quenching effect, which affirmed that the synthesized CQDs are selective for Cr^{6+} ions. Further sensitivity tests were carried out using a 1 μM stock solution of Cr^{6+} ions.

Plausible Reason for the CQD High Selectivity with Cr^{6+} Ions. The possible reason for the PL quenching of CQDs with the addition of Cr^{6+} ions is because of the high redox potential (~+1.33 V) of Cr^{6+} (eq 4) at acidic pH (since the inherent pH of the CQDs is 3.5), making it a strong oxidant which can be reduced in the presence of an electron donor moiety, *i.e.*, CQDs.[61] In water, Cr^{6+} exists in various anionic forms such as $Cr_2O_7^{2-}$, CrO_4^{2-}, and $HCrO_4^-$. These Cr^{6+} anionic forms are converted to each other as the pH of solution changes. $Cr_2O_7^{2-}$ and CrO_4^{2-} are in equilibrium in the solution, and as the solution becomes acidic, the reaction equilibrium moves toward left (eq 2), and as shown in eq 3, $Cr_2O_7^{2-}$ is instantaneously converted to $HCrO_4^-$ as the primary constituent.

$$Cr_2O_7^{2-} + H_2O \leftrightarrow 2CrO_4^{2-} + 2H^+ \quad (2)$$

$$Cr_2O_7^{2-} + H^+ \rightarrow 2HCrO_4^- + 2H_2O \quad (3)$$

$$HCrO_4^- + 7H^+ + 3e^- \rightarrow Cr(III) + 4H_2O \quad (E^0 = 1.33\ V) \quad (4)$$

The CQD surface contains profuse number of functional groups like hydroxyl, carboxyl, amide, and carbonyl, some of which have reduced capabilities. As a result, Cr^{6+} directly reduced to Cr^{3+} in the presence of CQDs.[62] The effect of pH on the performance of the sensors for the selective detection of Cr^{6+} was also studied. The sensor showed the maximum fluorescence quenching of Cr^{6+} in the acidic pH (Figure S5a).

Method of Validation. This method was authenticated in accordance with ICHQ2(R1) recommendations.[63]

Linearity and Range. The interaction of PL intensity of varied Cr^{6+} ion concentrations (nM range) with CQDs was tested to determine the sensitivity of the as-prepared sensor. The CQD PL intensity was gradually quenched with different

https://doi.org/10.1021/acsomega.3c02474
ACS Omega 2023, 8, 22178−22189

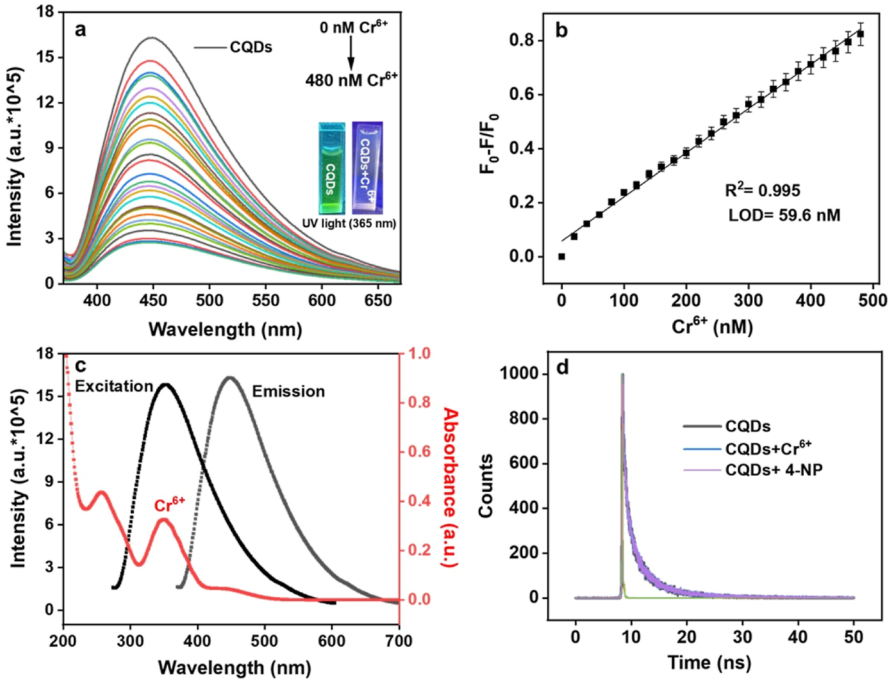

Figure 5. (a) Variation in the fluorescence intensity of CQDs with a distinct concentration of Cr^{6+} ions, (b) linear relation among PL response ($F_0 - F/F_0$) and Cr^{6+} ions (0−480 nM), (c) overlapping of absorption spectra of Cr^{6+} ions with the excitation and emission spectrum of CQDs, and (d) PL lifetime decay of CQDs with Cr^{6+} and 4-NP.

concentrations of Cr^{6+} ions, as exhibited in Figure 5a. To know the quenching efficacy, the Stern−Volmer plot was drawn using the following equation

$$\frac{F_0}{F} = 1 + K_{SV}[Q] \tag{5}$$

"F_0" and "F" are the CQD PL intensity in the absence and with the quencher, *i.e.*, Cr^{6+}. K_{SV} denotes the Stern−Volmer quenching constant. Figure S3a depicts the linear range of F_0/F and the Cr^{6+} concentrations (0−480 nM) with the regression equation as

$$\frac{F_0}{F} = 0.00626[Cr^{6+}] + 0.8514 \qquad (R^2 = 0.991) \tag{6}$$

The values of R^2 are approximate to unity, indicating the satisfactory linearity of the developed method.

Limit of Detection and Limit of Quantification. The detection limit for Cr^{6+} ions was calculated using $3\sigma/K$ and LOQ using $10\sigma/K$, where σ denotes the intercept's standard deviation, and K tells the slope of linear line. The LOD was calculated from Figure 5b, *i.e.*, 59.6 nM from a plot among PL responses ($F_0 - F/F_0$) and concentrations of Cr^{6+} ions (0−480 nM) with R^2 = 0.995. Table 1 shows the LOQ value of 198.7 nM.

Table 2 displays that the developed sensors have high sensitivity toward Cr^{6+} ions compared to other sensors mentioned in the literature.

Binding Efficiency. To determine the binding interaction and stoichiometry between CQDs and Cr^{6+}, the excited-state binding constant was estimated with a 1:1 linear Benesi−Hildebrand (B−H) equation

$$\frac{1}{F_0 - F} = \frac{1}{F_0 - F_1} + \frac{1}{K[Q](F_0 - F)} \tag{7}$$

"F_0" and "F" signifies the PL intensities in the absence and with Cr^{6+}. "Q" denotes the quencher concentration. F_1 is the intensity of 1:1 stoichiometric CQDs−Cr^{6+}. "K" denotes the values of binding constant of CQDs with Cr^{6+}. The plot between $(1/F_0 - F)$ *versus* $1/[Q]$ exhibits a linear line with K = 602 nM^{-1} and R^2 = 0.997 (Figure S3b and Table 1).

Table 1. Sensing Capabilities for Cr^{6+} by the Prepared Sensor

parameters	Cr^{6+}
range	0−480 nM
limit of detection[a]	59.6 nM
limit of quantification[b]	198.7 nM
regression equation	$F_0/F = 0.00626[Cr^{6+}] + 0.8514$
binding efficacy	602 nM^{-1}
K_{SV}	0.00626 nM^{-1}

[a]LOD = $3\sigma/K$. [b]LOQ = $10\sigma/K$, σ is intercept's standard deviation, and K represents slope.

Table 2. Different Quantum Dot-Based Sensing Devices for Cr^{6+} Detection

sr. no.	the sensor system	linearity range	detection limit	refs
1	CQDs	0.5−200 μM	0.73 μM	43
2	N-CQDs	0−100 μM	2.1 μM	39
3	CQDs	1−20 μM	0.175 μM	42
4	N,S-CQDs	1−10 μM	0.2 μM	64
5	N,S-CQDs	1−40 μM	0.52 μM	65
6	B,N-CDs	0.3−500 μM	0.24 μM	66
7	CQDs	0−480 nM	59.6 nM	current work

Analysis of Precision. An experiment was done to know the intra-day and inter-day precisions, which was carried out with three distinct concentrations along with three replicas of each concentration. Allowed % RSD value was <2%, demonstrating that the prepared method has acceptable precision (Table S1).

Sensitivity Studies for the Detection of Cr^{6+}. The linear response range and sensitivity of CQDs for Cr^{6+} ions were calculated by adding distinct concentrations of Cr^{6+} ions (0−

https://doi.org/10.1021/acsomega.3c02474
ACS Omega 2023, 8, 22178−22189

480 nM) under optimized conditions. Figure 5a clearly shows that with a gradual increase in Cr^{6+} concentrations, the CQD intensity was gradually decreased. Figure S3a shows the decent linear response of F_0/F with the concentration of Cr^{6+} by regression eq 6 having a 0.991 correlation coefficient. The detection limit was found to be 59.6 nM (Figure 5b), which is much lower than the reported sensitivity parameter value in the previous literature (Table 2), since the average lifetime data of the as-prepared CQD remains constant in the existence of Cr^{6+} (Table S2), which clearly depicts that the developed inner filter effect (IFE)-based fluorescence sensor has a high sensitivity to detect Cr^{6+} ions offering benefits like fast implementation, facile, and expediency.

Analysis of Real Samples. Table 3 depicts the practicability of CQDs toward sensing of Cr^{6+} ions in lake water and tap water.

Table 3. Application of the Developed Sensor for the Detection of Cr^{6+} in Real Samples

sample	added (μM)	found (μM)	recovery (%)	RSD (%)
lake water	0.5	0.47	94.80	1.23
	1.5	1.51	100.6	1.32
	2.5	2.48	99.20	1.06
	5	4.94	98.80	0.30
tap water	0.5	0.46	92.0	1.24
	1.5	1.48	98.6	0.67
	2.5	2.51	100.4	1.79
	5	4.93	98.6	0.42

The data showed the good recovery percentage and relative standard deviation (% RSD). The observed values exhibited the acceptable precision values, confirming that the as-prepared CQDs can be successfully used for the sensing of Cr^{6+} in the real water samples.

Possible Fluorescence Sensing Mechanism of Cr^{6+}. To examine the plausible interaction mechanism of Cr^{6+} ions and CQDs, the optical properties of the spectra of Cr^{6+} and CQDs were first studied to know the quenching mechanism. Figure 5c shows the excitation and emission spectra of CQDs and UV−vis spectra of Cr^{6+}. Here, the maximum absorption peak of the quencher, *i.e.*, Cr^{6+}, was overlapped with the excitation spectra of CQDs, which is due to the IFE. It is a decent spectral overlay among the absorber's absorption band with the fluorophore's excitation/emission band.[43] As shown in Figure 5c, Cr^{6+} showed the broad absorption peak at 257, 352, and 444 nm. Simultaneously, CQDs displayed an excitation band at 360 nm with an emission peak centered at 448 nm, demonstrating a great amount of effective overlapping between the excitation, emission, and absorption bands in the developed sensing system. Henceforth, the PL quenching can be credited to the IFE.[67] Also, the PL decay spectrum of CQDs without and with Cr^{6+} were further studied to validate the quenching mechanism. As depicted in Figure 5d, the average lifetimes of CQDs and CQDs + Cr^{6+} were 1.086 and 1.106 ns, respectively (Table S2). The minimal change in the fluorescence lifetimes after the Cr^{6+} addition denotes that there was no substantial electron transfer between CQDs and Cr^{6+}, and the mechanism was ascribed to IFE (Scheme 2).[37]

DETECTION OF 4-NP

Selectivity of CQD toward 4-NP. To study the selectivity of fabricated CQDs toward 4-NP, changes in CQDs PL intensity were studied in the existence of various analytes like glucose, HQ, AA, 4-NP, 2-NP, glycine, EDTA, alanine, glutathione (GSH), MP, nitrobenzene, 1-fluoro 2-nitrobenzene (1-F-2NB), and phenol. Figure 6a depicts that the PL quenching efficiency of CQDs was maximum in the case of 4-NP than the remaining analytes. This displayed the excellent selectivity of synthesized CQDs toward 4-NP. The fluorescence quenching can be accredited to the energy transfer amid CQDS and 4-NP.[68] Also, the overlap among the absorption spectra of 4-NP with the excitation and emission spectra of CQDs was responsible for PL quenching. As depicted in Scheme 3, the energy transfer could be eased by establishment of a zwitterionic spirocyclic Meisenheimer complex through CQDs and 4-NP combination. The negative charge gets delocalized across the cyclohexadiene ring and the nitro group as a consequence of the creation of a Meisenheimer complex, while a positive charge will spread on the iminium group. This transfer of energy produced by localization of charges leads to fluorescence quenching of

Scheme 2. Plausible Sensing Mechanism of Cr^{6+}

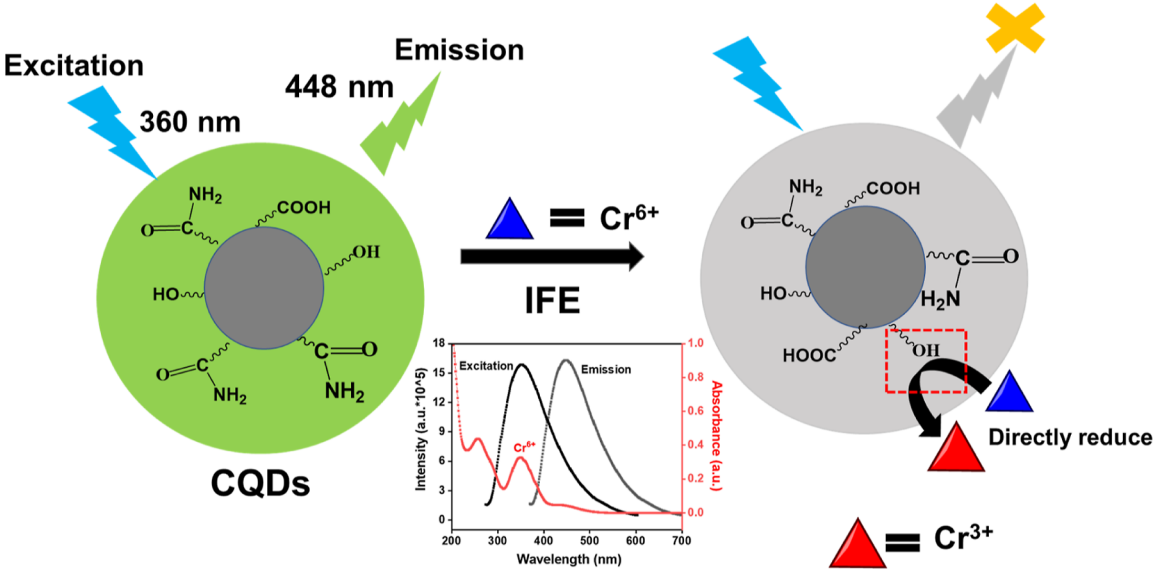

https://doi.org/10.1021/acsomega.3c02474
ACS Omega 2023, 8, 22178−22189

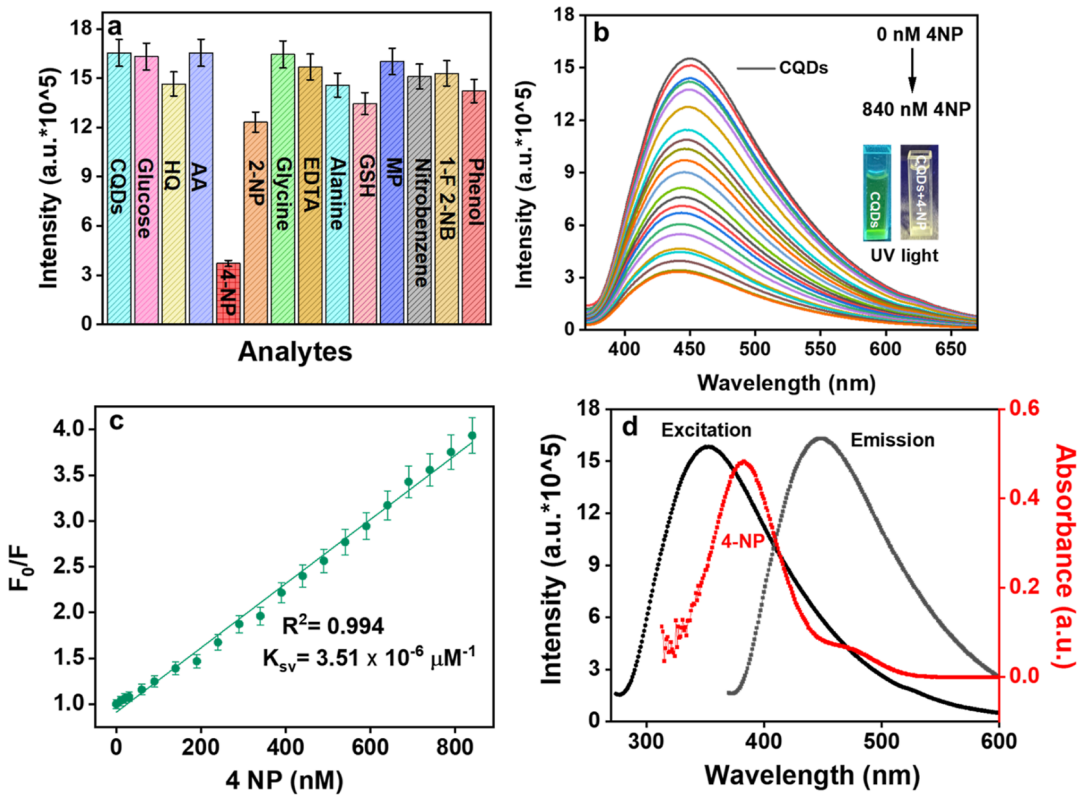

Figure 6. (a) Interference analysis of CQDs for 4-NP ions, (b) change in PL intensity of CQDs with distinct concentrations of 4-NP ions, (c) linear relation amid PL response (F_0/F) and 4-NP concentrations, and (d) overlapping of 4-NP absorption spectrum with CQD excitation and emission spectrum.

Scheme 3. Plausible Quenching Mechanism of CQDs in the Presence of 4-NP

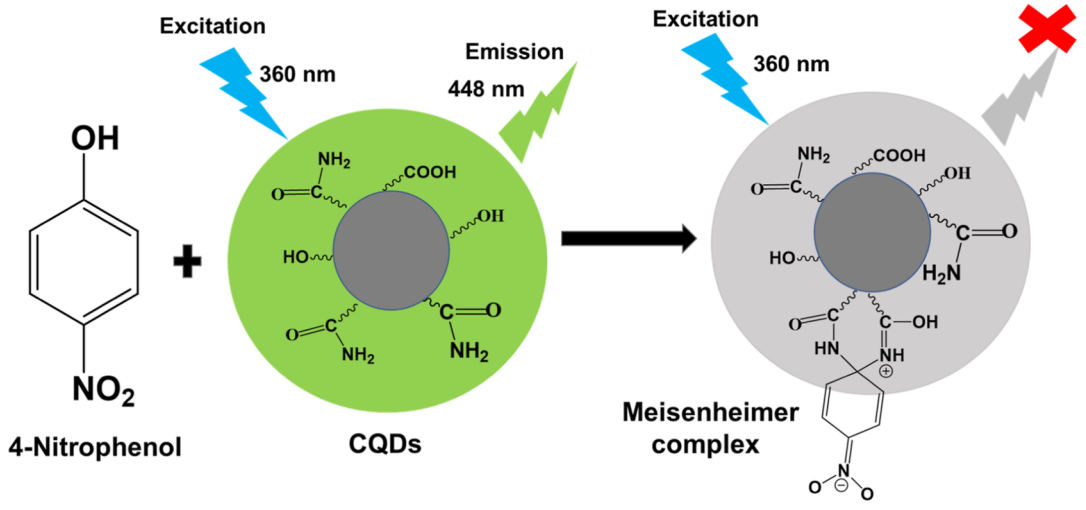

CQDs. Further sensitivity tests were carried out with a 1 μM stock solution of 4-NP. The effect of pH on the performance of the sensors for the selective detection of 4-NP was also carried out. The sensor showed the maximum fluorescence quenching of 4-NP in the basic pH (Figure S5b).

Sensitivity Studies of 4-NP. The PL intensity of the fabricated CQDs was eventually quenched by gradually adding various concentrations of 4-NP (0−840 nM) (Figure 6b). The detection limit (LOD), linearity range, LOQ, and further analytical parameters are tabulated in Table 4. Figure S4a shows the linear relation among PL responses ($F_0 - F/F_0$) and different concentrations of 4-NP (0−840 nM) with the inset figure showing the linear calibration curve between $F_0 - F/F_0$ and concentration of 4-NP (0−90 nM) having a correlation coefficient of 0.991. The limit of detection was 14 nM, which was calculated using the IUPAC criterion ($3\sigma/K$), which is lower as compared to the values stated in the previous literature studies (Table 5). The linear calibration curve was derived from the Stern−Volmer graph with the regression equation F_0/F = 0.00351[4-NP] + 0.91171, here F_0 and F are the PL intensity of CQDs without and with 4-NP with the high correlation coefficient (R^2 = 0.994) (Figure 6c). The binding efficacy was

https://doi.org/10.1021/acsomega.3c02474
ACS Omega 2023, 8, 22178−22189

Table 4. Analytical Performance for 4-NP by the Prepared Sensor

parameters	4-NP
linearity range	0−90 nM
limit of detection[a]	14 nM
limit of quantification[b]	63.8 nM
regression equation	$F_0/F = 0.00351[4\text{-NP}] + 0.91171$
binding efficacy	8403 nM^{-1}
K_{SV}	0.00351 nM^{-1}

[a]LOD = $3\sigma/K$. [b]LOQ = $10\sigma/K$, σ is intercept's standard deviation and K denotes the slope.

Table 5. Different Sensors for 4-NP Detection

sr. no.	sensor system	linearity range	detection limit	refs
1	carbon dots (CDs)	0.1−50 μM	0.028 μM	69
2	B,N-CDs	0.5−200 μM	0.20 μM	70
3	β-CDs@ZnO QDs	1.0−40 μM	0.34 μM	71
4	CdTe QDs	1.0−30 μM	40 nM	26
5	CDs	0.001−1 μM	60 nM	60
6	CQDs	0−90 nM	14 nM	current work

also calculated using eq 7. The graph between $(1/F_0 - F)$ *vs* $1/[Q]$ depicts a linear line showing $K = 8403\ nM^{-1}$ and $R^2 = 0.992$ (Figure S4b and Table 4). Precision analysis was also performed with the acceptable % RSD value of less than 2%, indicating that the developed method had an acceptable precision (Table S1). Real sample analysis was also carried out to confirm the practicability of the developed sensor against the detection of 4-NP in the real water samples. The result showed good % RSD and recoveries (Table S3).

Quenching Mechanism. The PL quenching mechanism of CQDs in the presence of 4-NP can be elucidated by the spectral overlapping of the absorption spectra of acceptor, *i.e.*, 4-NP, with the excitation and emission spectra of donor, *i.e.*, CQDs. This is because of the IFE as depicted in Figure 6d, the absorption spectra of 4-NP is at 378 nm, which was overlapped with the excitation peak of CQDs that is cantered at 360 nm.[72] The PL decay spectra of CQDs with and without 4-NP were further evaluated to check the quenching mechanism. Figure 4d shows that the average lifetimes of CQDs and CQDs + 4-NP were 1.086 and 1.078 ns, respectively (Table S2). Also, the zwitterionic spirocyclic Meisenheimer complex formation was responsible (Scheme 3). Here, the nitro group and the cyclohexadiene ring contain the negative charge, and the iminium group comprises the positive charge.[73] The transfer of energy created by the charge localization might lead to substantial fluorescence quenching of CQDs upon addition of 4-NP (contact quenching).[51]

CONCLUSIONS

In the current work, an eco-friendly, green methodology, and cheaper approach was used for the synthesis of highly water-soluble fluorescent CQDs from biomass waste (orange pomace) by the microwave irradiation without incorporation of chemical substituents. The synthesized CQDs are stable, green luminescent, showing excitation-dependent emission ranging from 300 to 420 nm. CQDs act as a nanosensor for the sensitive detection of Cr^{6+} with 82% quenching and a detection limit of 59.6 nM within the concentration range of 0−480 nM. The PL quenching was attributed to IFE. Also, the prepared CQDs were applied for the detection of the extremely important mono-nitrophenols with respect to environmental concern. CQDs reacted well toward 4-NP with 14 nM LOD in the 0−90 nM concentration range. This is possibly because of the formation of the zwitterionic spirocyclic Meisenheimer complex and IFE. Validation of the as-prepared sensor was performed in accordance with ICH recommendations. Moreover, the developed method was used to effectively detect chromium (Cr^{6+}) and 4-NP in real water samples with acceptable % RSD and precision. This current method and the detection strategy comes out to be a cheaper, easier, and environment-friendly approach for the detection of Cr^{6+} and 4-NP for various applications.

ASSOCIATED CONTENT

Supporting Information

The Supporting Information is available free of charge at https://pubs.acs.org/doi/10.1021/acsomega.3c02474.

Characterizations; precision data for the detection of Cr^{6+}, 4-NP by the fabricated sensor; lifetime parameters of CQDs, CQDs + Cr^{6+}, and CQDs + 4-NP; application of the developed sensor for the detection of 4-NP in real samples; zeta potential and pH studies of CQDs; selectivity of CQDs using different metal anions; Stern−Volmer quenching graph of CQDs with Cr^{6+}; B−H binding graph of CQDs with Cr^{6+}; linear relation among PL response $(F_0 - F/F_0)$ and 4-NP different concentrations; binding (B−H) graph of CQDs with 4-NP; and effect of pH on the performance of the sensors for the selective detection of Cr^{6+} and 4-NP (PDF)

AUTHOR INFORMATION

Corresponding Authors

Banibrata Maity − *School of Chemistry and Biochemistry, Affiliate Faculty—TIET-Virginia Tech Center of Excellence in Emerging Materials, Thapar Institute of Engineering and Technology, Patiala 147004, India;* orcid.org/0000-0003-0286-9028; Email: banibrata.maity@thapar.edu

Soumen Basu − *School of Chemistry and Biochemistry, Affiliate Faculty—TIET-Virginia Tech Center of Excellence in Emerging Materials, Thapar Institute of Engineering and Technology, Patiala 147004, India;* orcid.org/0000-0001-6419-1326; Email: soumen.basu@thapar.edu

Author

Aayushi Kundu − *School of Chemistry and Biochemistry, Senior Research Fellow—TIET-Virginia Tech Center of Excellence in Emerging Materials, Thapar Institute of Engineering and Technology, Patiala 147004, India;* orcid.org/0000-0002-1435-5078

Complete contact information is available at: https://pubs.acs.org/10.1021/acsomega.3c02474

Notes

The authors declare no competing financial interest.

ACKNOWLEDGMENTS

A.K. is grateful to TIET-VT Center of Excellence in Emerging Materials (CEEMS) for fellowship. The authors are grateful to IIT Roorkee for XPS analysis. The authors are thankful to CIL, PU, Chandigarh, for HR-TEM analysis. The authors are truly grateful to SPMS, TIET, Patiala, for XRD and Raman analysis.

REFERENCES

(1) Das, R.; Bandyopadhyay, R.; Pramanik, P. Carbon Quantum Dots from Natural Resource: A Review. *Mater. Today Chem.* **2018**, *8*, 96−109.

(2) Đorđević, L.; Arcudi, F.; Cacioppo, M.; Prato, M. A Multifunctional Chemical Toolbox to Engineer Carbon Dots for Biomedical and Energy Applications. *Nat. Nanotechnol.* **2022**, *17*, 112−130.

(3) Atchudan, R.; Jebakumar Immanuel Edison, T. N.; Shanmugam, M.; Perumal, S.; Somanathan, T.; Lee, Y. R. Sustainable Synthesis of Carbon Quantum Dots from Banana Peel Waste Using Hydrothermal Process for in Vivo Bioimaging. *Phys. E* **2021**, *126*, 114417.

(4) Zhu, L.; Shen, D.; Wang, Q.; Luo, K. H. Green Synthesis of Tunable Fluorescent Carbon Quantum Dots from Lignin and Their Application in Anti-Counterfeit Printing. *ACS Appl. Mater. Interfaces* **2021**, *13*, 56465−56475.

(5) Sohal, N.; Maity, B.; Basu, S. Morphology-Dependent Performance of MnO2Nanostructure-Carbon Dot-Based Biosensors for the Detection of Glutathione. *ACS Appl. Bio Mater.* **2021**, *4*, 5158−5168.

(6) Taghipour, S.; Jannesari, M.; Taghipour, M.; Ataie-Ashtiani, B.; Akhavan, O. Synthesis and Application of Carbon-Based Nanomaterials for Bioelectrochemical Systems. In *Advanced Nanomaterials and Nanocomposites for Bioelectrochemical Systems*; Elsevier, 2023; pp 327−356.

(7) Jalilinejad, N.; Rabiee, M.; Baheiraei, N.; Ghahremanzadeh, R.; Salarian, R.; Rabiee, N.; Akhavan, O.; Zarrintaj, P.; Hejna, A.; Saeb, M. R.; Zarrabi, A.; Sharifi, E.; Yousefiasl, S.; Zare, E. N. Electrically Conductive Carbon-Based (Bio)-Nanomaterials for Cardiac Tissue Engineering. *Bioeng. Transl. Med.* **2023**, *8*, No. e10347.

(8) Lim, S. Y.; Shen, W.; Gao, Z. Carbon Quantum Dots and Their Applications. *Chem. Soc. Rev.* **2015**, *44*, 362−381.

(9) Khan, Z. M. S. H.; Rahman, R. S.; Shumaila; Islam, S.; Zulfequar, M. Hydrothermal Treatment of Red Lentils for the Synthesis of Fluorescent Carbon Quantum Dots and Its Application for Sensing Fe3+. *Opt. Mater.* **2019**, *91*, 386−395.

(10) Wang, C.; Shi, H.; Yang, M.; Yan, Y.; Liu, E.; Ji, Z.; Fan, J. Facile Synthesis of Novel Carbon Quantum Dots from Biomass Waste for Highly Sensitive Detection of Iron Ions. *Mater. Res. Bull.* **2020**, *124*, 110730.

(11) Thangaraj, B.; Solomon, P. R.; Chuangchote, S.; Wongyao, N.; Surareungchai, W. Biomass-derived Carbon Quantum Dots−A Review. Part 1: Preparation and Characterization. *ChemBioEng Rev.* **2021**, *8*, 265−301.

(12) Tayyebi, A.; Akhavan, O.; Lee, B.-K.; Outokesh, M. Supercritical Water in Top-down Formation of Tunable-Sized Graphene Quantum Dots Applicable in Effective Photothermal Treatments of Tissues. *Carbon* **2018**, *130*, 267−272.

(13) Jouyandeh, M.; Tavakoli, O.; Sarkhanpour, R.; Sajadi, S. M.; Zarrintaj, P.; Rabiee, N.; Akhavan, O.; Lima, E. C.; Saeb, M. R. Green Products from Herbal Medicine Wastes by Subcritical Water Treatment. *J. Hazard. Mater.* **2022**, *424*, 127294.

(14) Borna, S.; Sabzi, R. E.; Pirsa, S. Synthesis of Carbon Quantum Dots from Apple Juice and Graphite: Investigation of Fluorescence and Structural Properties and Use as an Electrochemical Sensor for Measuring Letrozole. *J. Mater. Sci.: Mater. Electron.* **2021**, *32*, 10866−10879.

(15) Sun, C.; Zhang, Y.; Wang, P.; Yang, Y.; Wang, Y.; Xu, J.; Wang, Y.; Yu, W. W. Synthesis of Nitrogen and Sulfur Co-Doped Carbon Dots from Garlic for Selective Detection of Fe3+. *Nanoscale Res. Lett.* **2016**, *11*, 110.

(16) Li, Z.; Zhang, Y.; Niu, Q.; Mou, M.; Wu, Y.; Liu, X.; Yan, Z.; Liao, S. A Fluorescence Probe Based on the Nitrogen-Doped Carbon Dots Prepared from Orange Juice for Detecting Hg2+ in Water. *J. Lumin.* **2017**, *187*, 274−280.

(17) Schneider, E. M.; Bärtsch, A.; Stark, W. J.; Grass, R. N. Safe One-Pot Synthesis of Fluorescent Carbon Quantum Dots from Lemon Juice for a Hands-on Experience of Nanotechnology. *J. Chem. Educ.* **2019**, *96*, 540−545.

(18) Chatzimitakos, T.; Kasouni, A.; Sygellou, L.; Avgeropoulos, A.; Troganis, A.; Stalikas, C. Two of a Kind but Different: Luminescent Carbon Quantum Dots from Citrus Peels for Iron and Tartrazine Sensing and Cell Imaging. *Talanta* **2017**, *175*, 305−312.

(19) Tovar, A. K.; Godínez, L. A.; Espejel, F.; Ramírez-Zamora, R. M.; Robles, I. Optimization of the Integral Valorization Process for Orange Peel Waste Using a Design of Experiments Approach: Production of High-Quality Pectin and Activated Carbon. *Waste Manage.* **2019**, *85*, 202−213.

(20) Akhavan, O.; Bijanzad, K.; Mirsepah, A. Synthesis of Graphene from Natural and Industrial Carbonaceous Wastes. *RSC Adv.* **2014**, *4*, 20441−20448.

(21) Gustavsson, J.; Cederberg, C.; Sonesson, U. *Global Food Losses and Food Waste*; UNEP, FAO: Rome, 2011; p 1.

(22) Granucci, N.; Harris, P. J.; Villas-Boas, S. G. Chemical Compositions of Fruit and Vegetable Pomaces from the Beverage Industries. *Waste Biomass Valorization* **2023**, 1−16.

(23) Luo, X.; Bai, P.; Wang, X.; Zhao, G.; Feng, J.; Ren, H. Preparation of Nitrogen-Doped Carbon Quantum Dots and Its Application as a Fluorescent Probe for Cr (VI) Ion Detection. *New J. Chem.* **2019**, *43*, 5488−5494.

(24) Lv, R.; Wang, J.; Zhang, Y.; Li, H.; Yang, L.; Liao, S.; Gu, W.; Liu, X. An Amino-Decorated Dual-Functional Metal−Organic Framework for Highly Selective Sensing of Cr (III) and Cr (VI) Ions and Detection of Nitroaromatic Explosives. *J. Mater. Chem. A* **2016**, *4*, 15494−15500.

(25) US Department of Health and Human Services. *Toxicological Profile for Chromium*; Public Health Service Agency for Toxic Substances and Diseases Registry: Washington, DC, 1991.

(26) Jiang, L.; Liu, H.; Li, M.; Xing, Y.; Ren, X. Surface Molecular Imprinting on CdTe Quantum Dots for Fluorescence Sensing of 4-Nitrophenol. *Anal. Methods* **2016**, *8*, 2226−2232.

(27) Wang, M.; Gao, M.; Deng, L.; Kang, X.; Yang, L.; Quan, T.; Xia, Z.; Gao, D. Composite Material Based on Carbon Dots and Molecularly Imprinted Polymers: A Facile Probe for Fluorescent Detection of 4-Nitrophenol. *Nano* **2020**, *15*, 2050105.

(28) Arancibia, V.; Valderrama, M.; Silva, K.; Tapia, T. Determination of Chromium in Urine Samples by Complexation−Supercritical Fluid Extraction and Liquid or Gas Chromatography. *J. Chromatogr. B: Anal. Technol. Biomed. Life Sci.* **2003**, *785*, 303−309.

(29) Galeano-Díaz, T.; Guiberteau-Cabanillas, A.; Mora-Díez, N.; Parrilla-Vázquez, P.; Salinas-López, F. Rapid and Sensitive Determination of 4-Nitrophenol, 3-Methyl-4-Nitrophenol, 4, 6-Dinitro-o-Cresol, Parathion-Methyl, Fenitrothion, and Parathion-Ethyl by Liquid Chromatography with Electrochemical Detection. *J. Agric. Food Chem.* **2000**, *48*, 4508−4513.

(30) Anthemidis, A. N.; Zachariadis, G. A.; Kougoulis, J.-S.; Stratis, J. A. Flame Atomic Absorption Spectrometric Determination of Chromium (VI) by on-Line Preconcentration System Using a PTFE Packed Column. *Talanta* **2002**, *57*, 15−22.

(31) Hussain, S.; Muhammad Junaid, H.; Tahir Waseem, M.; Rauf, W.; Jabbar Shaikh, A.; Anjum Shahzad, S. Aggregation-Induced Emission of Quinoline Based Fluorescent and Colorimetric Sensors for Rapid Detection of Fe3+ and 4-Nitrophenol in Aqueous Medium. *Spectrochim. Acta, Part A* **2022**, *272*, 121021.

(32) Ravindran, A.; Elavarasi, M.; Prathna, T. C.; Raichur, A. M.; Chandrasekaran, N.; Mukherjee, A. Selective Colorimetric Detection of Nanomolar Cr (VI) in Aqueous Solutions Using Unmodified Silver Nanoparticles. *Sens. Actuators, B* **2012**, *166−167*, 365−371.

(33) Li, L.-L.; Feng, X.-Q.; Han, R.-P.; Zang, S.-Q.; Yang, G. Cr (VI) Removal via Anion Exchange on a Silver-Triazolate MOF. *J. Hazard. Mater.* **2017**, *321*, 622−628.

(34) Hu, S.; Xu, C.; Wang, G.; Cui, D. Voltammetric Determination of 4-Nitrophenol at a Sodium Montmorillonite-Anthraquinone Chemically Modified Glassy Carbon Electrode. *Talanta* **2001**, *54*, 115−123.

(35) Jin, W.; Wu, G.; Chen, A. Sensitive and Selective Electrochemical Detection of Chromium (VI) Based on Gold Nanoparticle-Decorated Titania Nanotube Arrays. *Analyst* **2014**, *139*, 235−241.

(36) Li, J.; Kuang, D.; Feng, Y.; Zhang, F.; Xu, Z.; Liu, M. A Graphene Oxide-Based Electrochemical Sensor for Sensitive Determination of 4-Nitrophenol. *J. Hazard. Mater.* **2012**, *201−202*, 250−259.

https://doi.org/10.1021/acsomega.3c02474
ACS Omega 2023, 8, 22178−22189

(37) Feng, S.; Gao, Z.; Liu, H.; Huang, J.; Li, X.; Yang, Y. Feasibility of Detection Valence Speciation of Cr (III) and Cr (VI) in Environmental Samples by Spectrofluorimetric Method with Fluorescent Carbon Quantum Dots. *Spectrochim. Acta, Part A* **2019**, *212*, 286−292.
(38) Kundu, A.; Maity, B.; Basu, S. Coal-Derived Graphene Quantum Dots with a Mn2+/Mn7+ Nanosensor for Selective Detection of Glutathione by a Fluorescence Switch-off-on Assay. *New J. Chem.* **2022**, *46*, 7545−7556.
(39) Wang, G.; Zhang, S.; Cui, J.; Gao, W.; Rong, X.; Lu, Y.; Gao, C. Preparation of Nitrogen-Doped Carbon Quantum Dots from Chelating Agent and Used as Fluorescent Probes for Accurate Detection of ClO− and Cr(VI). *Anal. Chim. Acta* **2022**, *1195*, 339478.
(40) Xu, Z.; Liu, J.; Wang, K.; Yan, B.; Hu, S.; Ren, X.; Gao, Z. Facile Synthesis of N-Doped Carbon Dots for Direct/Indirect Detection of Heavy Metal Ions and Cell Imaging. *Environ. Sci. Pollut. Res.* **2021**, *28*, 19878−19889.
(41) Guo, Y.; Chen, Y.; Cao, F.; Wang, L.; Wang, Z.; Leng, Y. Hydrothermal Synthesis of Nitrogen and Boron Doped Carbon Quantum Dots with Yellow-Green Emission for Sensing Cr (VI), Anti-Counterfeiting and Cell Imaging. *RSC Adv.* **2017**, *7*, 48386−48393.
(42) Mondal, T. K.; Mondal, S.; Ghorai, U. K.; Saha, S. K. White Light Emitting Lanthanide Based Carbon Quantum Dots as Toxic Cr (VI) and PH Sensor. *J. Colloid Interface Sci.* **2019**, *553*, 177−185.
(43) Li, L.; Shao, C.; Wu, Q.; Wang, Y.; Liu, M. Green Synthesis of Multifunctional Carbon Nanodots and Their Applications as a Smart Nanothermometer and Cr(VI) Ions Sensor. *Nano* **2018**, *13*, 1850147.
(44) Das, D.; Dutta, R. K. N-Doped Carbon Dots Synthesized from Ethylene Glycol and *β*-Alanine for Detection of Cr(VI) and 4-Nitrophenol via Photoluminescence Quenching. *ACS Appl. Nano Mater.* **2021**, *4*, 3444−3454.
(45) Huang, X.; Yang, C.; Chen, Y.; Zhu, Z.; Zhou, L. Cuttlefish Ink-Based N and S Co-Doped Carbon Quantum Dots as a Fluorescent Sensor for Highly Sensitive and Selective Para-Nitrophenol Detection. *Anal. Methods* **2021**, *13*, 5351−5359.
(46) Amjadi, M.; Hallaj, T. Dramatic Enhancement Effect of Carbon Quantum Dots on the Chemiluminescence of Ru (Bpy) 32+−Ce (IV) Reaction and Application to the Determination of 4-Nitrophenol. *J. Lumin.* **2016**, *171*, 202−207.
(47) Demasa, J. N.; Crosby, G. A. The Measurement of Photo-luminescence Quantum Yields. 1 A Review2. *J. Chem. Phys.* **1968**, *48*, 4726.
(48) Kainth, S.; Goel, N.; Basu, S.; Maity, B. Surfactant-Derived Water-Soluble Carbon Dots for Quantitative Determination of Fluoride via a Turn-off−on Strategy. *New J. Chem.* **2022**, *46*, 686−694.
(49) Guo, Y.; Zhao, W. Hydrothermal Synthesis of Highly Fluorescent Nitrogen-Doped Carbon Quantum Dots with Good Biocompatibility and the Application for Sensing Ellagic Acid. *Spectrochim. Acta, Part A* **2020**, *240*, 118580.
(50) Hu, X.; Li, Y.; Xu, Y.; Gan, Z.; Zou, X.; Shi, J.; Huang, X.; Li, Z.; Li, Y. Green One-Step Synthesis of Carbon Quantum Dots from Orange Peel for Fluorescent Detection of Escherichia Coli in Milk. *Food Chem.* **2021**, *339*, 127775.
(51) Dang, D. K.; Sundaram, C.; Ngo, Y. L. T.; Choi, W. M.; Chung, J. S.; Kim, E. J.; Hur, S. H. Pyromellitic Acid-Derived Highly Fluorescent N-Doped Carbon Dots for the Sensitive and Selective Determination of 4-Nitrophenol. *Dyes Pigm.* **2019**, *165*, 327−334.
(52) Singh, V. K.; Singh, V.; Yadav, P. K.; Chandra, S.; Bano, D.; Kumar, V.; Koch, B.; Talat, M.; Hasan, S. H. Bright-Blue-Emission Nitrogen and Phosphorus-Doped Carbon Quantum Dots as a Promising Nanoprobe for Detection of Cr(vi) and Ascorbic Acid in Pure Aqueous Solution and in Living Cells. *New J. Chem.* **2018**, *42*, 12990−12997.
(53) Sahu, S.; Behera, B.; Maiti, T. K.; Mohapatra, S. Simple One-Step Synthesis of Highly Luminescent Carbon Dots from Orange Juice: Application as Excellent Bio-Imaging Agents. *Chem. Commun.* **2012**, *48*, 8835−8837.
(54) Akhavan, O. Bacteriorhodopsin as a Superior Substitute for Hydrazine in Chemical Reduction of Single-Layer Graphene Oxide Sheets. *Carbon* **2015**, *81*, 158−166.
(55) Thambiraj, S.; Ravi Shankaran, D. Green Synthesis of Highly Fluorescent Carbon Quantum Dots from Sugarcane Bagasse Pulp. *Appl. Surf. Sci.* **2016**, *390*, 435−443.
(56) Mewada, A.; Pandey, S.; Shinde, S.; Mishra, N.; Oza, G.; Thakur, M.; Sharon, M.; Sharon, M. Green Synthesis of Biocompatible Carbon Dots Using Aqueous Extract of Trapa Bispinosa Peel. *Mater. Sci. Eng., C* **2013**, *33*, 2914−2917.
(57) Calizo, I.; Balandin, A. A.; Bao, W.; Miao, F.; Lau, C. N. Temperature Dependence of the Raman Spectra of Graphene and Graphene Multilayers. *Nano Lett.* **2007**, *7*, 2645−2649.
(58) Lv, P.; Yao, Y.; Zhou, H.; Zhang, J.; Pang, Z.; Ao, K.; Cai, Y.; Wei, Q. Synthesis of Novel Nitrogen-Doped Carbon Dots for Highly Selective Detection of Iron Ion. *Nanotechnology* **2017**, *28*, 165502.
(59) Kundu, A.; Maity, B.; Basu, S. Rice Husk-Derived Carbon Quantum Dots-Based Dual-Mode Nanoprobe for Selective and Sensitive Detection of Fe3+and Fluoroquinolones. *ACS Biomater. Sci. Eng.* **2022**, *8*, 4764−4776.
(60) Qu, Y. Y.; Ren, G.; Yu, L.; Zhu, B.; Chai, F.; Chen, L. The Carbon Dots as Colorimetric and Fluorescent Dual-Readout Probe for 2-Nitrophenol and 4-Nitrophenol Detection. *J. Lumin.* **2019**, *207*, 589−596.
(61) Sun, Y.; Yue, Q.; Gao, B.; Gao, Y.; Li, Q.; Wang, Y. Adsorption of Hexavalent Chromium on Arundo Donax Linn Activated Carbon Amine-Crosslinked Copolymer. *Chem. Eng. J.* **2013**, *217*, 240−247.
(62) Yang, W.-M.; Liu, F.; Jin, Y.-T.; Dong, Z.-M.; Zhao, G.-C. Efficient Reduction of Cr (VI) with Carbon Quantum Dots. *ACS Omega* **2022**, *7*, 23555−23565.
(63) ICH Expert Working Group. *ICH Harmonised Tripartite Guideline. Validation of Analytical Procedures: Text and Methodology Q2 (R1)*, 2005; Vol. *1* (20), p 05.
(64) Zhang, H.; Huang, Y.; Hu, Z.; Tong, C.; Zhang, Z.; Hu, S. Carbon Dots Codoped with Nitrogen and Sulfur Are Viable Fluorescent Probes for Chromium (VI). *Microchim. Acta* **2017**, *184*, 1547−1553.
(65) Shen, J.; Shang, S.; Chen, X.; Wang, D.; Cai, Y. Highly Fluorescent N, S-Co-Doped Carbon Dots and Their Potential Applications as Antioxidants and Sensitive Probes for Cr (VI) Detection. *Sens. Actuators, B* **2017**, *248*, 92−100.
(66) Wang, Y.; Hu, X.; Li, W.; Huang, X.; Li, Z.; Zhang, W.; Zhang, X.; Zou, X.; Shi, J. Preparation of Boron Nitrogen Co-Doped Carbon Quantum Dots for Rapid Detection of Cr (VI). *Spectrochim. Acta, Part A* **2020**, *243*, 118807.
(67) Gong, X.; Liu, Y.; Yang, Z.; Shuang, S.; Zhang, Z.; Dong, C. An "on-off-on" Fluorescent Nanoprobe for Recognition of Chromium(VI) and Ascorbic Acid Based on Phosphorus/Nitrogen Dual-Doped Carbon Quantum Dot. *Anal. Chim. Acta* **2017**, *968*, 85−96.
(68) Hua, J.; Yang, J.; Zhu, Y.; Zhao, C.; Yang, Y. Highly Fluorescent Carbon Quantum Dots as Nanoprobes for Sensitive and Selective Determination of Mercury (II) in Surface Waters. *Spectrochim. Acta, Part A* **2017**, *187*, 149−155.
(69) Ahmed, G. H. G.; Laíño, R. B.; Calzón, J. A. G.; García, M. E. D. Highly Fluorescent Carbon Dots as Nanoprobes for Sensitive and Selective Determination of 4-Nitrophenol in Surface Waters. *Microchim. Acta* **2015**, *182*, 51−59.
(70) Xiao, N.; Liu, S. G.; Mo, S.; Li, N.; Ju, Y. J.; Ling, Y.; Li, N. B.; Luo, H. Q. Highly Selective Detection of P-Nitrophenol Using Fluorescence Assay Based on Boron, Nitrogen Co-Doped Carbon Dots. *Talanta* **2018**, *184*, 184−192.
(71) Geng, S.; Lin, S. M.; Liu, S. G.; Li, N. B.; Luo, H. Q. A New Fluorescent Sensor for Detecting: P -Nitrophenol Based on *β*-Cyclodextrin-Capped ZnO Quantum Dots. *RSC Adv.* **2016**, *6*, 86061−86067.
(72) Tammina, S. K.; Yang, Y. Highly Sensitive and Selective Detection of 4-Nitrophenol, and on-off-on Fluorescence Sensor for Cr (VI) and Ascorbic Acid Detection by Glucosamine Derived n-Doped Carbon Dots. *J. Photochem. Photobiol., A* **2020**, *387*, 112134.

https://doi.org/10.1021/acsomega.3c02474
ACS Omega 2023, 8, 22178−22189

(73) Bogale, R. F.; Chen, Y.; Ye, J.; Yang, Y.; Rauf, A.; Duan, L.; Tian, P.; Ning, G. Highly Selective and Sensitive Detection of 4-Nitrophenol and Fe3+ Ion Based on a Luminescent Layered Terbium (III) Coordination Polymer. *Sens. Actuators, B* **2017**, *245*, 171−178.

https://doi.org/10.1021/acsomega.3c02474
ACS Omega 2023, 8, 22178−22189